JOURNAL OF MATERIALS SCIENCE 20 (1985) 2903–2912

Structure and hardness of laser-processed Fe–0.2%C–5%Cr and Fe–0.2%C–10%Cr alloys

P. A. MOLIAN
Department of Mechanical Engineering, Iowa State University, Ames, Iowa 50011, USA

The effects of high quench rates achieved through a laser surface-alloying process on the martensitic transformations of Fe–0.2%C–Cr steels (up to 10 wt% chromium) were investigated. The microstructural variables: martensitic morphology and its substructure; amount of retained austenite; and carbide precipitation were characterized by optical metallography and thin foil transmission electron microscopy (TEM). The microstructures exhibited were fully lath martensitic type, the substructure of which consisted of dislocations. The morphology and substructure of martensite were influenced neither by the chromium content of the alloy nor by the laser parameters (or melt depth) employed. Thin films of retained austenite were observed at packet and lath boundaries of martensite and at prior austenite grain boundaries. The amount of retained austenite was found to decrease with decrease in melt depth. TEM studies also revealed the presence of more or less continuous cementite films both at the lath boundaries and within the laths. Microhardness measurements had shown that the hardness increased with increase in chromium content of the alloy but appeared to be independent of melt depth.

1. Introduction

Considerable work has been done on martensitic transformations and their influence on the resulting mechanical properties of carbon and alloy steels [1–20]. While the effects of carbon and substitutional alloying elements on the transformation substructures of martensites have been very well characterized and documented in the literature, relatively little emphasis has been attached to the relationship between quench or cooling rate and the resultant structure and properties of martensites. It has been known probably for a long time that cooling rate influences the extent of martensitic transformation. Mathews [12] observed increased amounts of retained austenite in oil-quenched steels over water-quenched steels. Klier and Troiano [13] reported an increase in M_s temperature with increase in quench rate for chromium steels. These results have stimulated many investigators [5–8] to seek to understand the effect of high quench rates on the relevant mechanisms of martensitic transformations. Donachie and Ansell [5] recently studied the effects of high quench rates (up to 4×10^4 °C sec^{-1}) on M_s temperature, percentage of austenite transformed, martensitic morphology and hardness. The results of their studies and other prior investigations [6–8] were explained on the basis of the degree of carbon segregation to structural imperfections in the austenite prior to the austenite–martensite transformation. However, the factors that control martensitic transformation behaviour at high quench rates have not yet been completely elucidated.

The current study of Fe–0.2 wt %C–Cr steels, produced through a laser surface-alloying process, has been directed at determining martensitic transformation behaviour as a function of composition (up to 10% chromium) and melt depth (100 to 1500 μm).

0022–2461/85 $03.00 + .12

TABLE I Laser beam parameters used in this study

Laser power	900 to 1200 W
Beam size	0.0066 to 0.040 cm
Scan rate	0.42 to 8.47 cm sec^{-1}
Lens	6.25 cm focal length (ZnSe)

2. Experimental procedure

Commercial low-carbon steel (C, 0.18 to 0.22%; Si, 0.08%; Mn, 0.68%; S, 0.010%; P, 0.07%), received in the form of cold-rolled steel bar, was vacuum degassed at 600° C and cut into specimens of size 7.5 cm × 2.5 cm × 0.64 cm. Chromium was then electrodeposited on these specimens using conventional plating methods. Chromium coating thickness was varied from 5 to 50 μm. After chromium deposition, the samples were again vacuum degassed (10^{-7} torr) at 205° C (400° F) to remove the entrapped hydrogen from the coating.

The chromium-deposited steels were then mounted on a numerically controlled x–y table and irradiated with a continuous high-power CO_2 laser beam of wavelength 10.6 μm. Different laser beam parameters were used (Table I) to obtain penetration depths from 100 to 1500 μm. Both single-scan and multiple-scan laser melting (successive laser passes were laid side by side) were employed. The cooling rates, estimated using solidification structures and heat transfer models [21–23], ranged from 10^3 to 10^6 ° C sec^{-1} depending on the melt depth. The desired alloy composition in the fusion zone was obtained by controlling the melt depth and initial chromium coating thickness.

Microstructural and compositional analysis consisted of optical microscopy, scanning electron microscopy (SEM), transmission electron microscopy (TEM), and energy-dispersive and and wavelength-dispersive X-ray microprobe analysis. Thin foils for TEM work were taken from the mid-regions of laser-alloyed zones. Slices of 0.6 mm thickness were mechanically sectioned, using flood cooling to avoid tempering. A series of 120, 240, 400 and 600 grit SiC papers were then used to reduce the thickness to 0.10 mm. Discs of 3 mm diameter were punched and thinned in a solution containing 5% perchloric acid in 2-butoxyethanol with 80 V applied voltage at −10° C using a twin jet polisher. The foils were then examined in a Hitachi HU- 11B electron microscope operated at 100 kV. For optical microscopy and SEM, the samples were polished and etched in 2% Nital and Villella's reagent. In addition to metallography, the fusion zone microhardness was determined using a Leitz miniload hardness tester.

3. Results and discussion

3.1. Laser-alloyed fusion zone studies

Fig. 1 shows transverse sections of laser-alloyed zones typically observed in single-laser-pass treated (Figs. 1a and b) and multiple-laser-pass treated (Figs. 1c and d) specimens. Compositional studies on laser-alloyed fusion zones revealed that the desired composition was obtained by controlling initial chromium coating thickness and penetration depth (Table II).

Uniform composition of laser-alloyed fusion zones was dependent upon the melt zone geometry. Studies by X-ray microprobe analysis indicated that uniform composition was achieved only in a semicircular melt zone (Figs. 1b and d). In contrast, deep penetration zones (Figs. 1a and c) contained composition gradients and these could be identified by the differences in etching behaviour within fusion zones. Microstructural and hardness studies were, however, made only on regions of uniform composition. Thin foil TEM work was carried out in transverse sections of multiple-laser-pass treated specimens.

TABLE II Laser alloying parameters (laser power, 1200 W)

Beam size (cm)	Scan rate (cm sec^{-1})	Nominal coating thickness (μm)	Penetration depth (μm)	Nominal composition (wt % Cr)
0.0066	2.11	50	1500	5
0.0254	4.66	20	600	5
0.0400	1.27	5	200	5
0.0066	5.50	50	1000	10
0.0254	4.66	35	600	10
0.0400	1.27	10	150	20

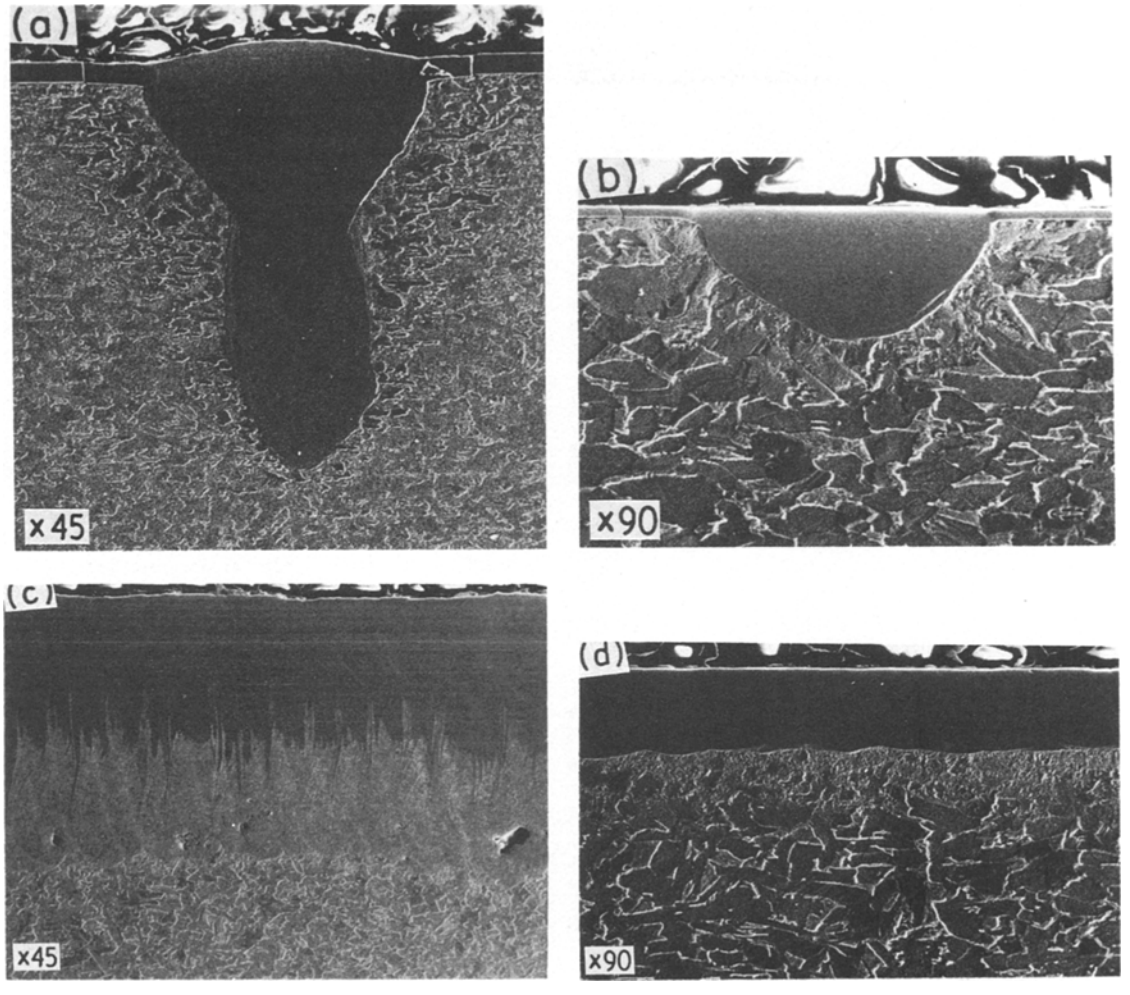

Figure 1 SEM micrographs of transverse sections of laser-alloyed zones: (a), (b) single laser pass; (c), (d) multiple laser pass.

3.2. Optical metallography

Figs. 2a to c are representative optical micrographs of laser-processed (single-pass) Fe–0.2%C–Cr alloys with different chromium contents. The as-quenched structures appear to be completely martensitic in nature. The columnar type of solidification structure is also evident. A comparison of Figs. 2a to c also shows that there is no apparent change in the morphology of martensite with increase in chromium content of the alloy. The same results were obtained for all melt depths. Fig. 3 is an optical micrograph of laser-processed (multiple-pass) 5% chromium alloy showing the martensitic structure with no columnar solidification structure. The disappearance of columnar structure is attributed to tempering of the fusion zone caused by successive overlapping passes.

3.3. Transmission electron microscopy

A detailed characterization of microstructures by TEM was performed on multiple-pass laser-melted 5 and 10% chromium alloys. These two alloys are representative compositions and can be utilized to predict the behaviour of other alloys within the γ-phase field of the Fe–Cr–C equilibrium diagram.

3.2.1. Martensitic substructure

TEM studies of 5 and 10% chromium alloys revealed a microstructure consisting of lath martensite occurring in packets. Figs. 4 and 5 illustrate the bright-field micrographs of 5 and 10% chromium alloys, respectively, for different melt depths. The laths were predominantly dislocated; however, some internal microtwinning in a few laths was also observed. Internal

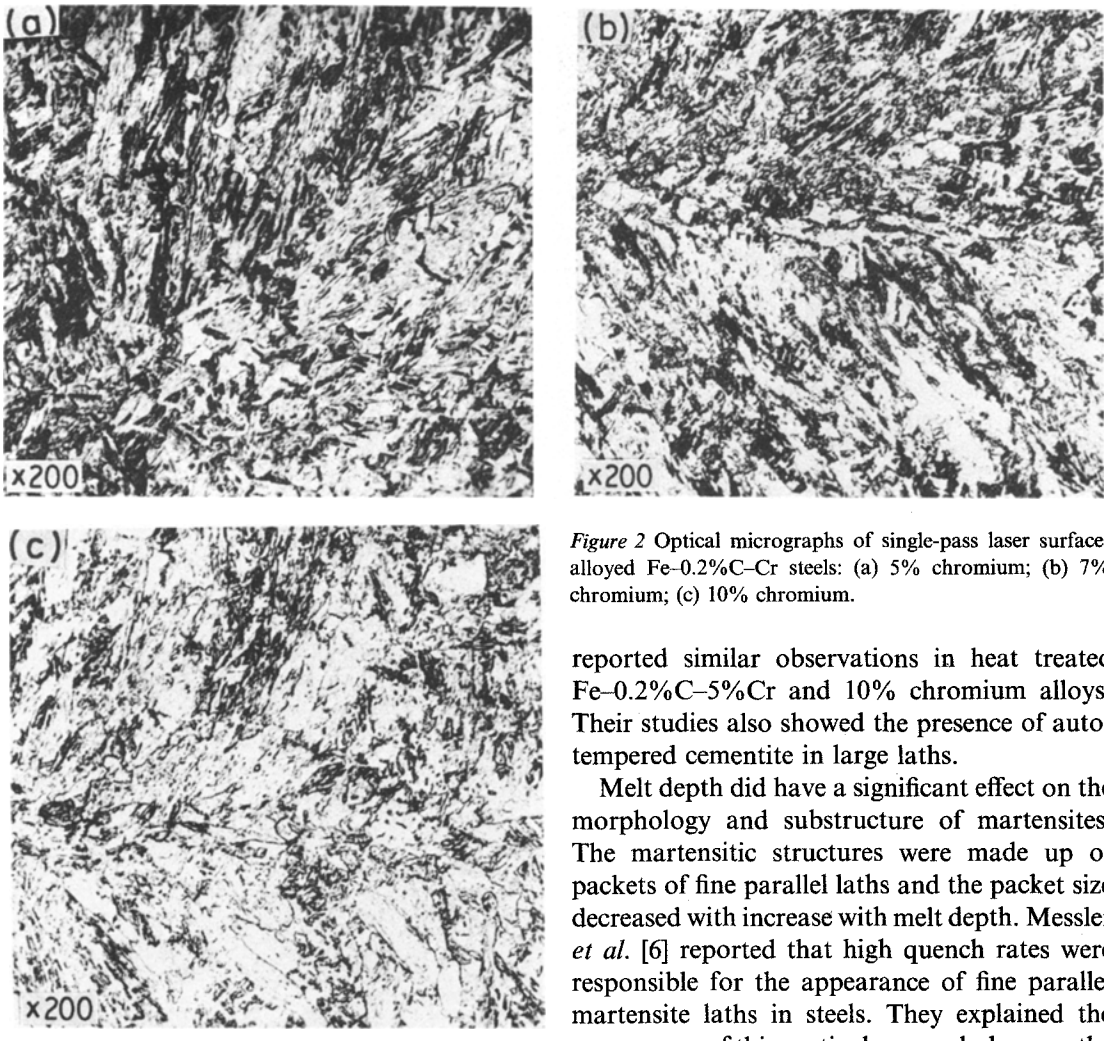

Figure 2 Optical micrographs of single-pass laser surface-alloyed Fe–0.2%C–Cr steels: (a) 5% chromium; (b) 7% chromium; (c) 10% chromium.

twinning in some individual laths has also been shown by many previous investigators for plain carbon and alloy steels [9, 14]. The laths within a packet of martensite were separated by low-angle boundaries, although in some regions twin related laths were also observed. Careful analysis of lath martensite structure indicated the presence of at least three types of lath morphologies: convergent laths; regular parallel laths and large laths containing extensive autotempered carbides. Regular parallel laths were most frequently observed with individual laths having planar boundaries (Figs. 4b and 5b). A convergent lath is occasionally observed within each martensite packet. Large laths containing autotempered carbides (Fig. 6a) were also observed and they most probably formed in the early stages of transformation. Howell *et al.* [4] reported similar observations in heat treated Fe–0.2%C–5%Cr and 10% chromium alloys. Their studies also showed the presence of autotempered cementite in large laths.

Melt depth did have a significant effect on the morphology and substructure of martensites. The martensitic structures were made up of packets of fine parallel laths and the packet size decreased with increase with melt depth. Messler *et al.* [6] reported that high quench rates were responsible for the appearance of fine parallel martensite laths in steels. They explained the appearance of this particular morphology on the

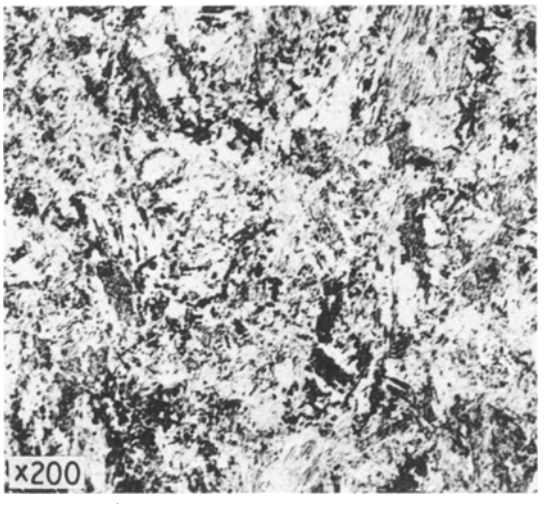

Figure 3 Optical micrograph of multiple-pass laser surface-alloyed Fe–0.2%C–5%Cr steel.

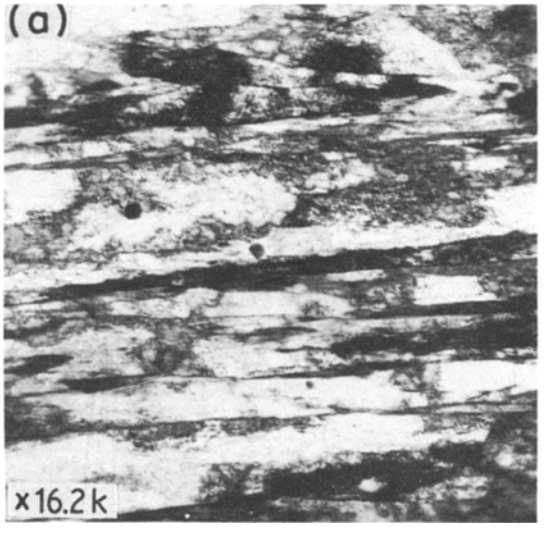

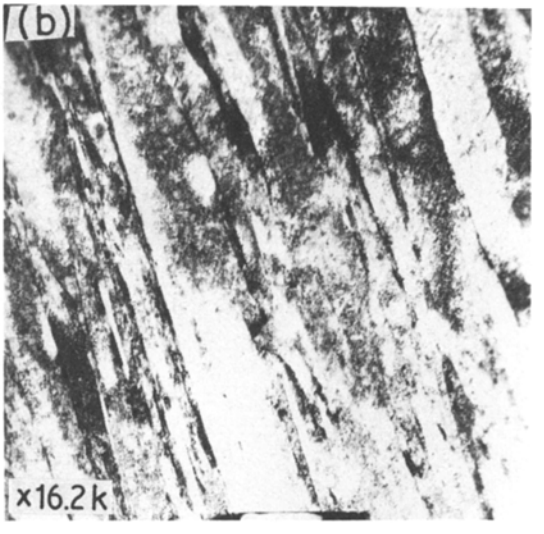

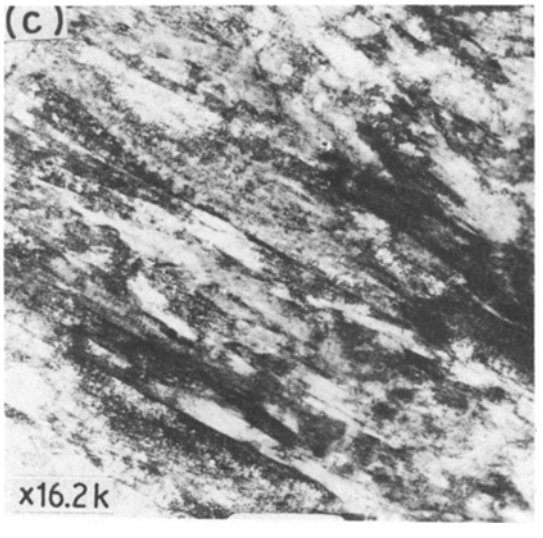

Figure 4 TEM micrographs of laser-processed 5% chromium alloy. Melt depth: (a) 1500 μm; (b) 600 μm; (c) 200 μm.

basis of the conditions under which growth takes place. The rate of quenching altered the growth morphology of martensite by changing the austenite shear strength through changes in the formation of carbon atmospheres at imperfections. Donachie and Ansell [5] observed twinned laths in fast-quenched (4×10^4 °C sec^{-1}) low-carbon steel. They attributed this change in morphology to a change in austenite shear strength caused by quench rate.

There was no change in the morphology and substructures of martensite observed between 5 and 10% chromium alloys. This suggests that the interaction between carbon and chromium (chromium reduces the diffusivity of carbon, thereby keeping it in solution) is not sufficient to induce changes in the M_s temperature or austenite shear strength, thereby causing the change in substructure. Kelly and Nutting [1] attributed the change in martensitic morphology and substructure to stacking fault energy and M_s temperature. Lowering M_s temperature or raising stacking fault energy should favour the formation of twinned martensite. Addition of chromium to a steel lowers the M_s temperature and also lowers the stacking fault energy, thereby producing opposing effects.

3.3.2. Retained austenite

TEM studies showed the existence of thin films of retained austenite at interlath boundaries and at prior austenite grain boundaries in laser-processed chromium steels. Figs. 6 and 7 illustrate the typical interlath film morphology of retained austenite for 5 and 10% chromium alloys. Analysis of SAD patterns, as illustrated in Figs. 6 an 7, revealed that the orientation relationship between the austenite and martensite was the Kurdjumov–Sachs (K–S) relationship, i.e. $(0\,1\,1)_\alpha \| (1\,1\,1)_\gamma$, $[1\,1\,1]_\alpha \| [1\,1\,0]_\gamma$, and the Nishiama–Wesserman (N–W) relationship, namely $(0\,0\,1)_\alpha \| (1\,1\,1)_\gamma$, $[1\,0\,0]_\alpha \| [1\,0\,1]_\gamma$.

The most significant conclusion in this study is that there is a decrease in the amount of retained austenite with decrease in melt depth. The largest amounts of retained austenite were observed in deep penetration melts. At this point, it is important to emphasize that the

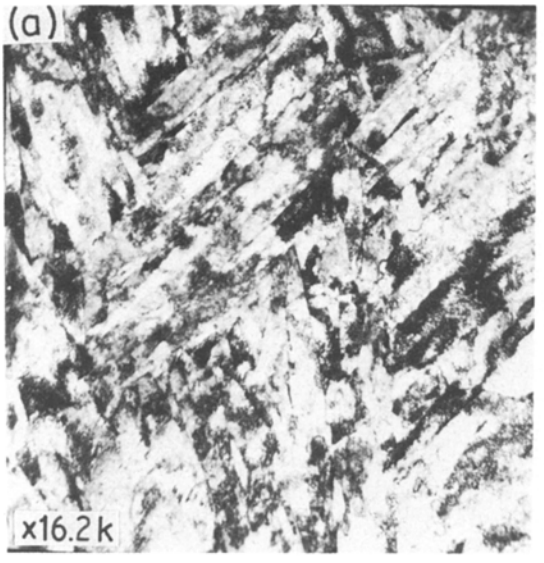

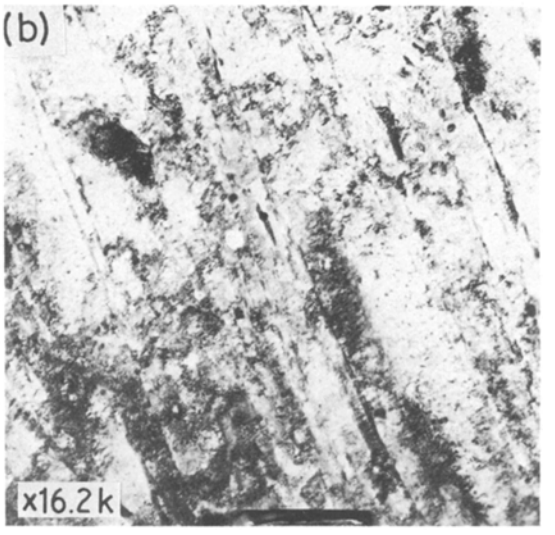

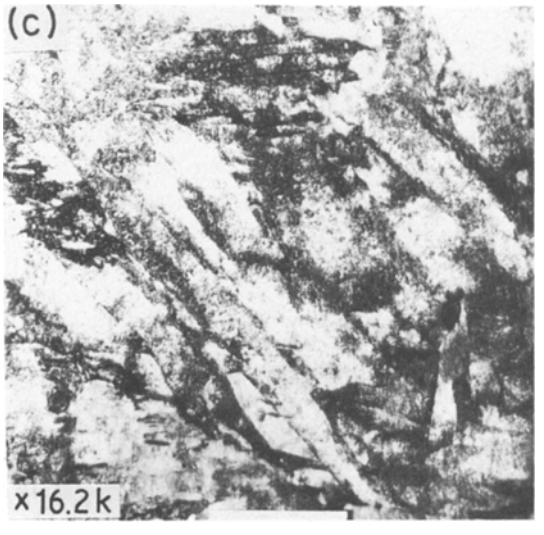

Figure 5 TEM micrographs of laser-processed 10% chromium alloy. Melt depth: (a) 1000 μm; (b) 600 μm; (c) 150 μm.

above conclusion is based upon the examination of a number of thin foils.

The presence of retained austenite in quenched steels is attributed to the following factors: (i) grain size, (ii) M_s temperature, (iii) carbide precipitation, (iv) austenite shear strength, and (v) alloy content. Several models have been proposed [5–8, 10, 11] to explain the stabilization of austenite at room temperature. They include chemical stabilization (carbon partitioning from lath martensite to the surrounding austenite during transformation or carbon–dislocation interactions inhibiting transformation), thermal stabilization (lowering M_s temperature) and mechanical stabilization (plastic deformation in austenite accompanying the shear transformation). The effect of melt depth in reducing the amount of retained austenite in the present study appears to be a combined effect of thermal and chemical stabilization. It is generally agreed [5–8] that M_s temperature increases with increase in quench rate. In terms of Ansell and Arrott's model [7], increasing quench rate decreases the time available for carbon segregation to structural imperfections in the austenite. As a result, the equilibrium carbon concentration in the carbon-defects atmosphere is not obtained. The austenite is no longer as effectively strengthened by the segregation of carbon to imperfections and the transformation to martensite can occur more easily. Thus, an increase in M_s temperature and reduction in austenite shear strength are probably responsible for the observed decrease in the amount of retained austenite with decreasing melt depth.

3.3.3. Carbide precipitation

Both ε-carbide and cementite were observed in all alloys irrespective of composition and cooling rate (Figs. 6c and 8). However, these carbides appear to be more pronounced in 5% than in 10% chromium alloy. The carbides were present both at the lath boundaries and within the laths. The shape and size of carbide particles was not influenced by quench rates. Carbide precipitation in these alloys is attributed to

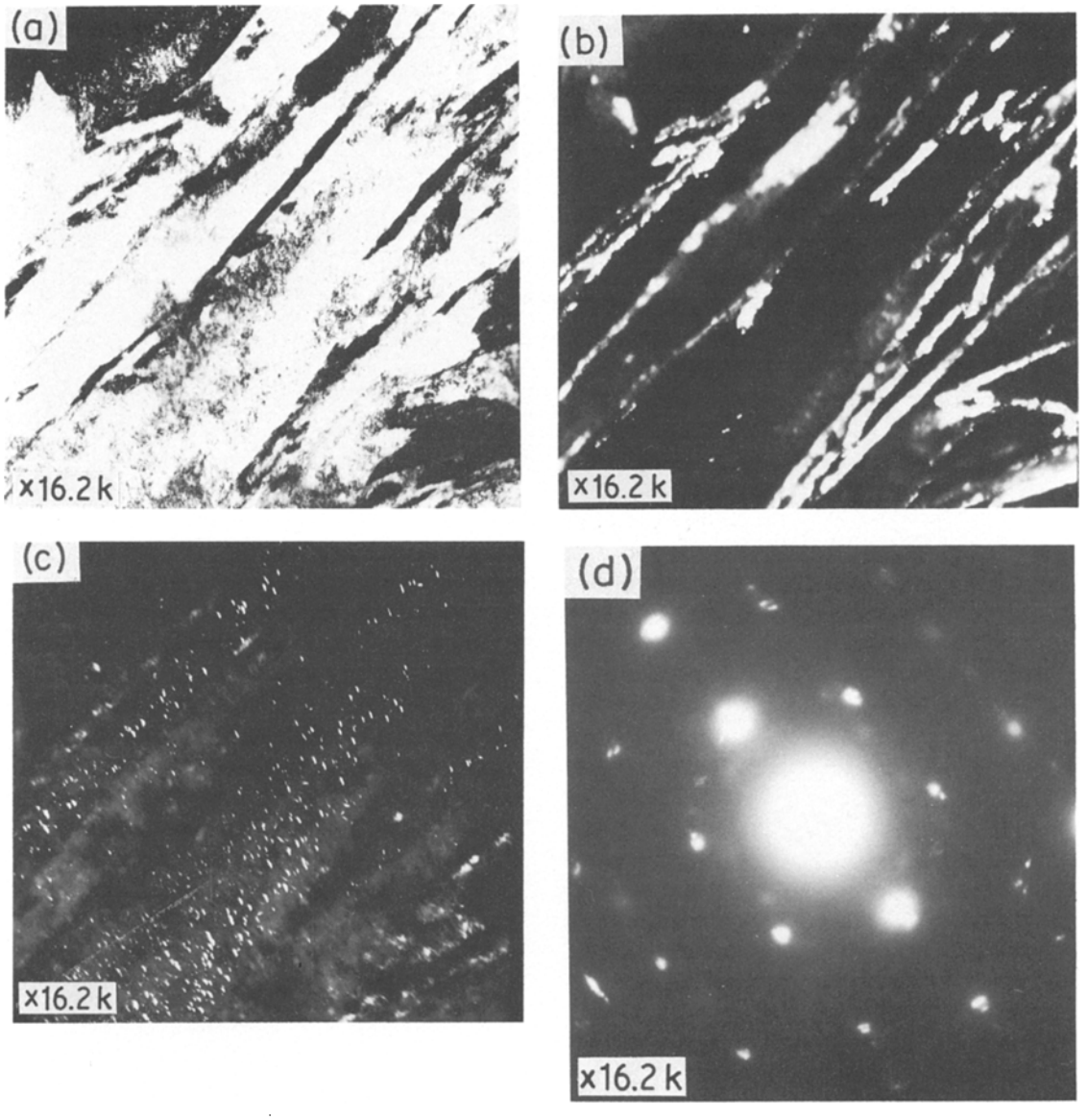

Figure 6 TEM micrographs of laser-processed 5% chromium alloy: (a) bright field; (b) dark field showing retained austenite; (c) dark field showing ε-carbide; (d) SAD pattern.

tempering of martensite caused by multiple scanning of the laser beam during this process.

3.4. Microhardness

Knoop microhardness studies were carried out on the fusion zones as functions of composition and penetration depth, both in single-pass and multiple-pass laser-melted alloys (Fig. 9). An increase in hardness was observed with increasing chromium content of the alloy but melt depth did not increase the hardness. High hardness in the high-chromium alloy is believed to be due to a substitutional solid-solution strengthening mechanism.

4. Conclusions

The microstructures and microhardness of the laser surface-alloyed Fe–0.2%C–Cr system have been investigated as functions of composition (up to 10% chromium) and melt depth (150–1500 μm). The structures were characterized by optical microscopy and thin-foil TEM.

The principal results and conclusions are as

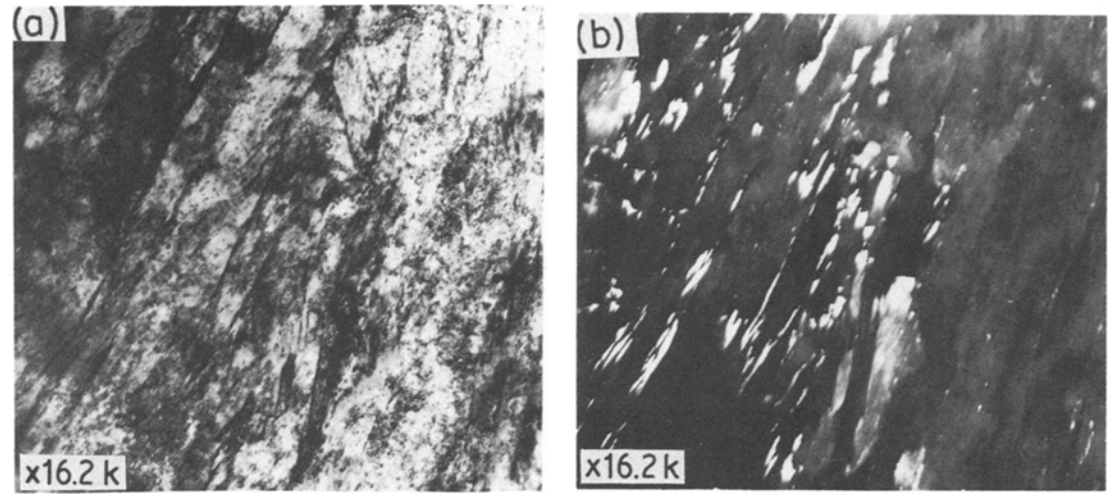

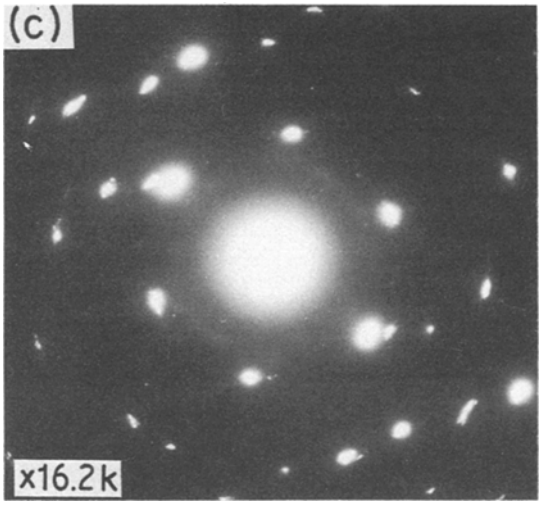

Figure 7 TEM micrographs of laser-processed 10% chromium alloy; (a) bright field; (b) dark field showing retained austenite; (c) SAD pattern.

follows:

1. The microstructures were essentially dislocated lath martensitic irrespective of composition and cooling rate.
2. Thin films of retained austenite were observed at lath packet boundaries of martensite and at prior austenite grain boundaries. The amounts of retained austenite were not influenced by composition but decreased with increase in cooling rate.
3. A homogeneous dispersion of ε-carbide

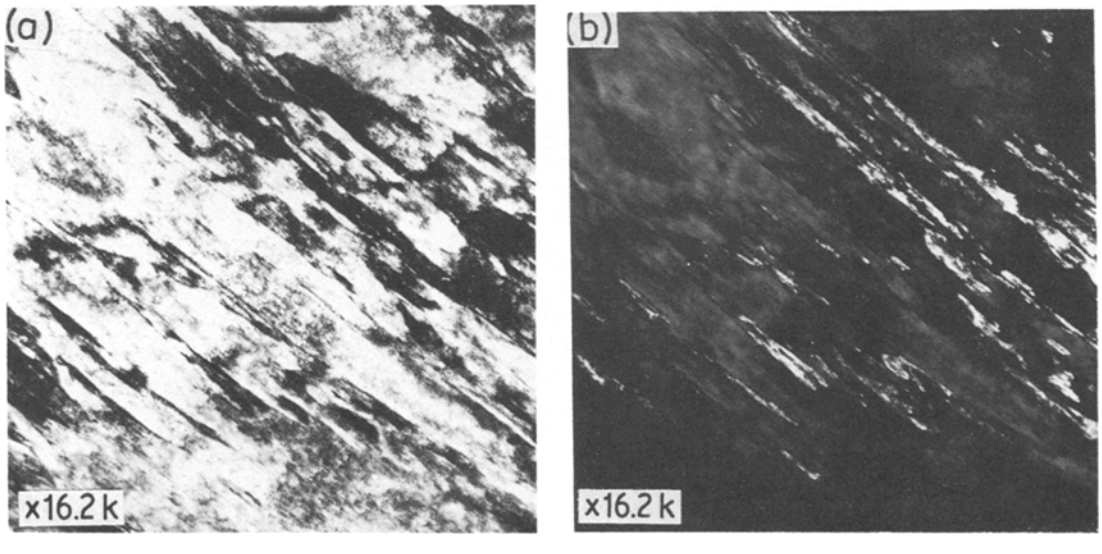

Figure 8 TEM micrographs of laser-processed 5% chromium alloy; (a), (c) bright fields; (b), (d) dark fields showing cementite.

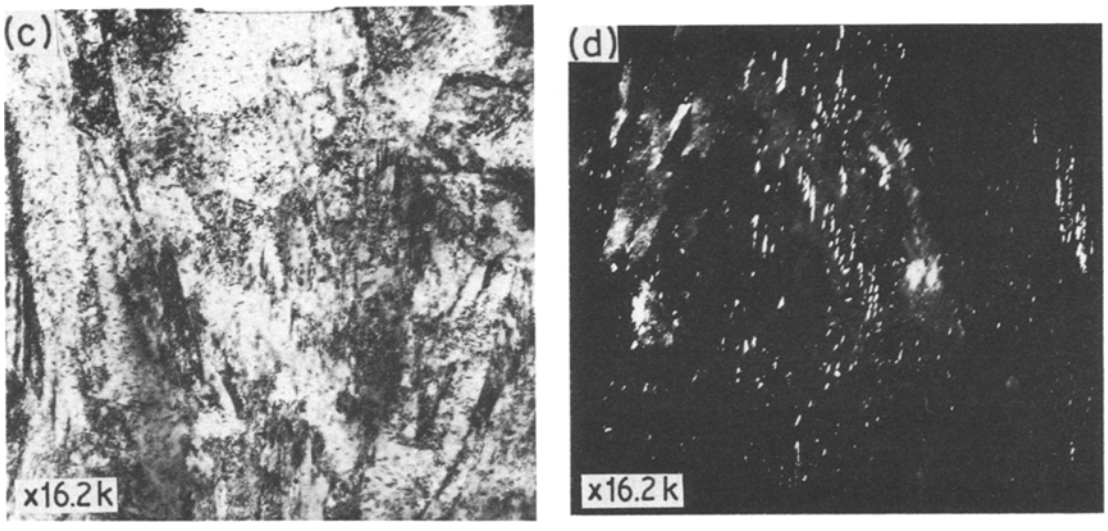

Figure 8 continued.

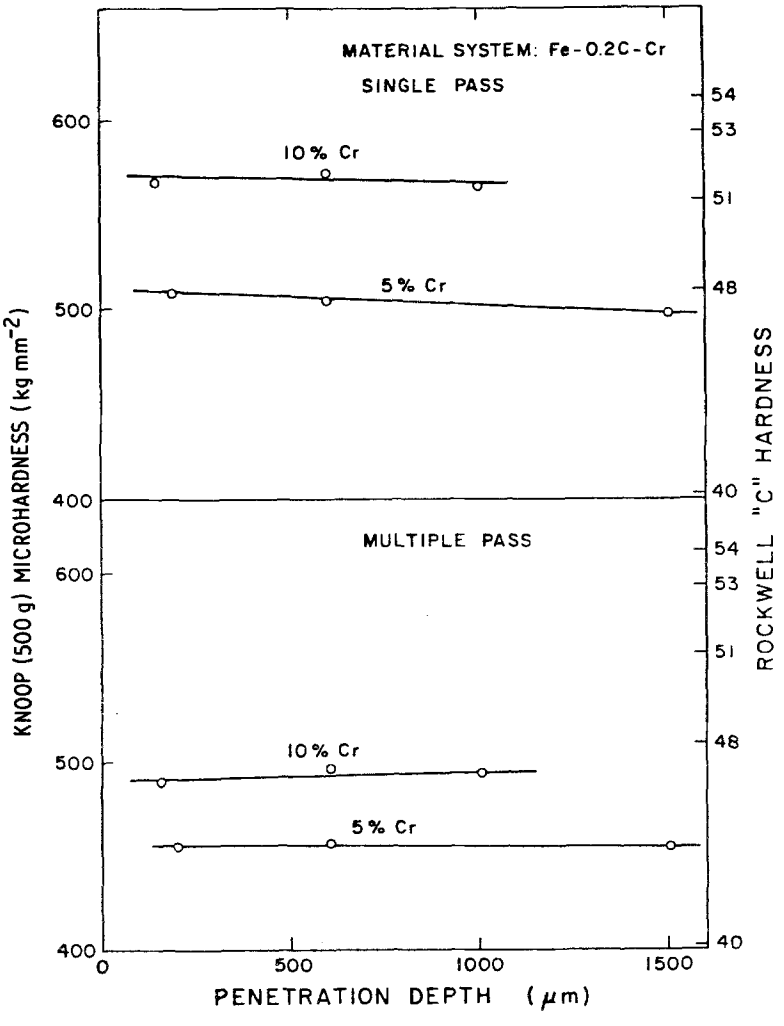

Figure 9 Effect of chromium content and melt depth on microhardness of laser-alloyed fusion zones.

and cementite, both at the lath boundaries and within laths, occurred in the martensite.

4. Chromium content of the fusion zone increased the hardness.

Acknowledgements

The author would like to thank Professor W. E. Wood for his suggestions and Oregon Graduate Center for providing facilities. This work was partially supported by the US Army Research Office.

References

1. P. M. KELLY and J. NUTTING, *J. Iron Steel Institute* (1961) 199.
2. G. KRAUSS and A. R. MARDER, *Met. Trans.* **2** (1971) 2343.
3. G. THOMAS, *ibid.* **2** (1971) 2373.
4. J. V. BEE, P. R. HOWELL and R. W. K. HONEYCOMBE, *ibid.* **10A** (1979) 1213.
5. D. S. J. DONACHIE and G. S. ANSELL, *ibid.* **6A** (1975) 1863.
6. R. W. MESSLER, G. S. ANSELL and V. I. LIZVNOV, *Trans. ASM* **62** (1969) 362.
7. G. S. ANSELL and A. ARROTT, *Trans. AIME* **227** (1963) 1080.
8. H. R. WOEHNLE, W. R. CLOUGH and G. S. ANSELL, *Trans. ASM* **59** (1966) 784.
9. S. K. DAS and G. THOMAS, *Met. Trans.* **1** (1970) 325.
10. B. V. N. RAO and G. THOMAS, *ibid.* **11A** (1980) 441.
11. G. THOMAS, *ibid.* **9A** (1978) 439.
12. J. A. MATHEWS, *Amer. Soc. Steel Treating* **8** (1925) 565.
13. E. P. KLIER and A. R. TROIANO, *Trans. AIME* **162** (1945) 175.
14. A. R. MARDER and G. KRAUS, *Trans. ASM* **60** (1967) 651.
15. B. V. N. RAO, T. Y. KOO and G. THOMAS, *Proc. Electron Microsc. Soc. Amer.* (1975) 30.
16. N. C. LAW, R. P. HOWELL and D. V. EDMONDS, *Met. Sci.* **13** (1979) 507.
17. S. CLARK and G. THOMAS, *Met. Trans.* **6A** (1975) 969.
18. E. M. BREINAN and G. S. ANSELL, *ibid.* **1** (1970) 1513.
19. C. M. WAYMAN, *ibid.* **1** (1970) 2009.
20. R. G. DAVIES and C. L. MAGEE, *ibid.* **1** (1970) 2927.
21. H. E. CLINE and T. R. ANTHONY, *J. Appl. Phys.* **48** (1977) 3895.
22. L. E. GREENWALD, E. M. BREINAN and B. H. KEAR, "Laser–Solid Interactions and Laser Processing–1978", edited by S. D. Ferris (American Institute of Physics, New York, 1979) p. 189.
23. W. E. BROWN, R. STRACHAN and M. C. FLEMINGS, *AFS Cast Met. Res. J.* (1970) 176.

Received 11 June
and accepted 20 September 1984